Supporting Information

Exploring structural, magnetic, and catalytic diversity in tetranuclear $\{Cu_4O_4\}$ cubane cores and a dinuclear complex derived from closely related ligand systems

Narayan Ch. Jana,[a] Albert Escuer,[b,c] Paula Brandão,[d] and Anangamohan Panja,[a,e,*]

[a] *Department of Chemistry, Panskura Banamali College, Panskura RS, WB 721152, India, India. E-mail: ampanja@yahoo.co.in*

[b] *Departament de Química Inorgànica i Orgànica, Secció de Química Inorgànica, Universitat de Barcelona, Marti i Franques 1-11, Barcelona-08028, Spain*

[c] *Institut de Nanociència i Nanotecnologia (IN^{2}UB), Universitat de Barcelona, Barcelona-08028, Spain.*

[d] *Department of Chemistry, CICECO-Aveiro Institute of Materials, University of Aveiro, 3810-193 Aveiro, Portugal*

[e] *Department of Chemistry, Gokhale Memorial Girls' College, 1/1 Harish Mukherjee Road, Kolkata-700020, India.*

Characteristic spectra of ligands

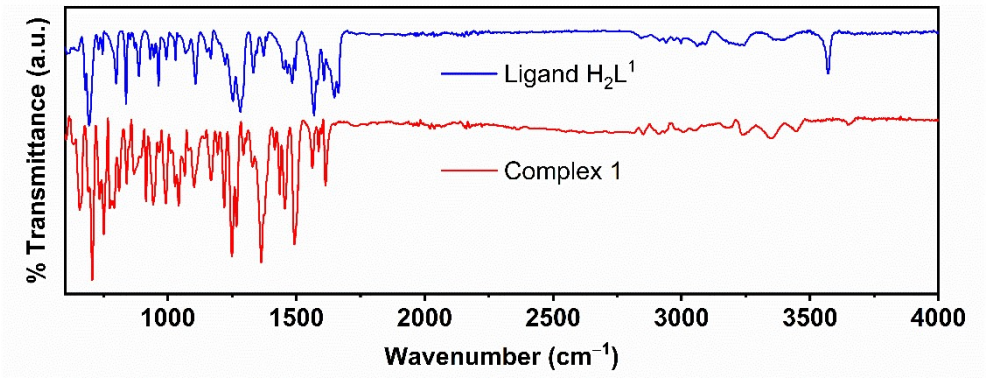

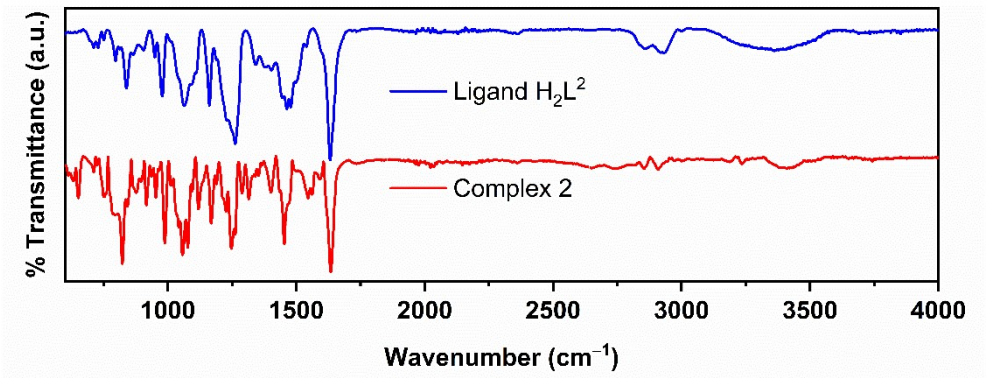

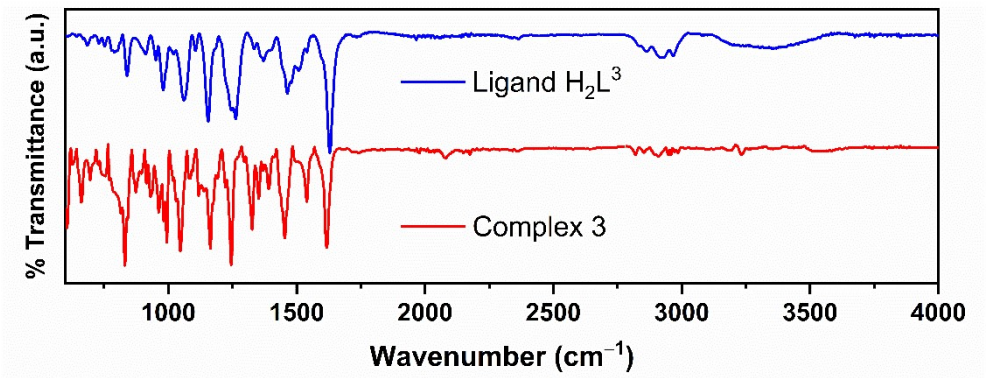

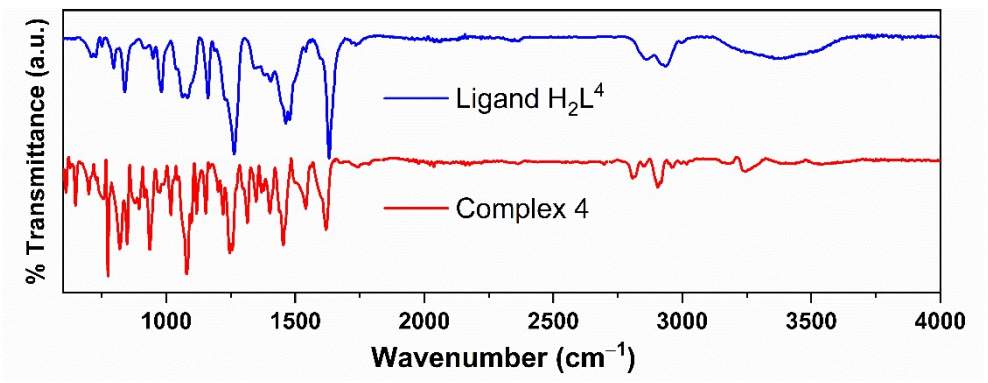

Fig. S1: FT-TR spectra of the four ligands and their corresponding complexes.

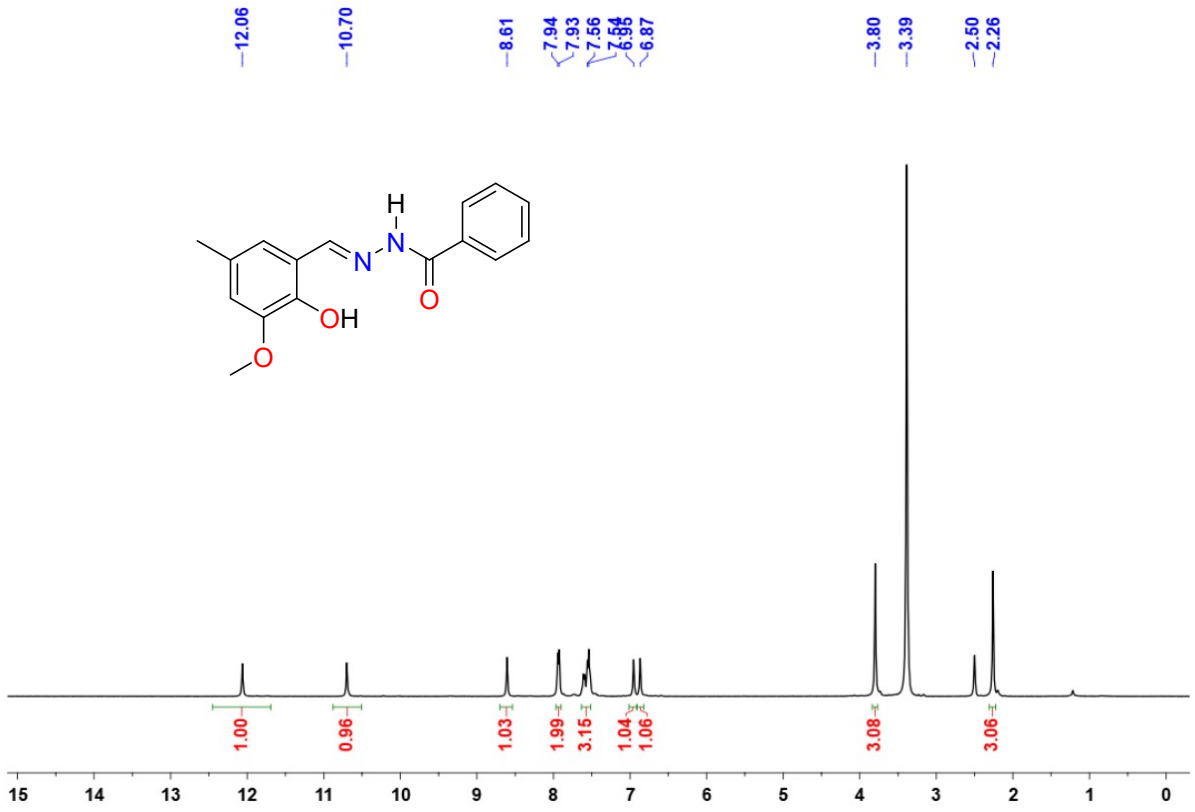

Fig. S2: ^{1}H NMR of *N*′-(2-hydroxy-3-methoxy-5-methylbenzylidene)benzohydrazide (H_2L^1) in DMSO d_6 at r.t.

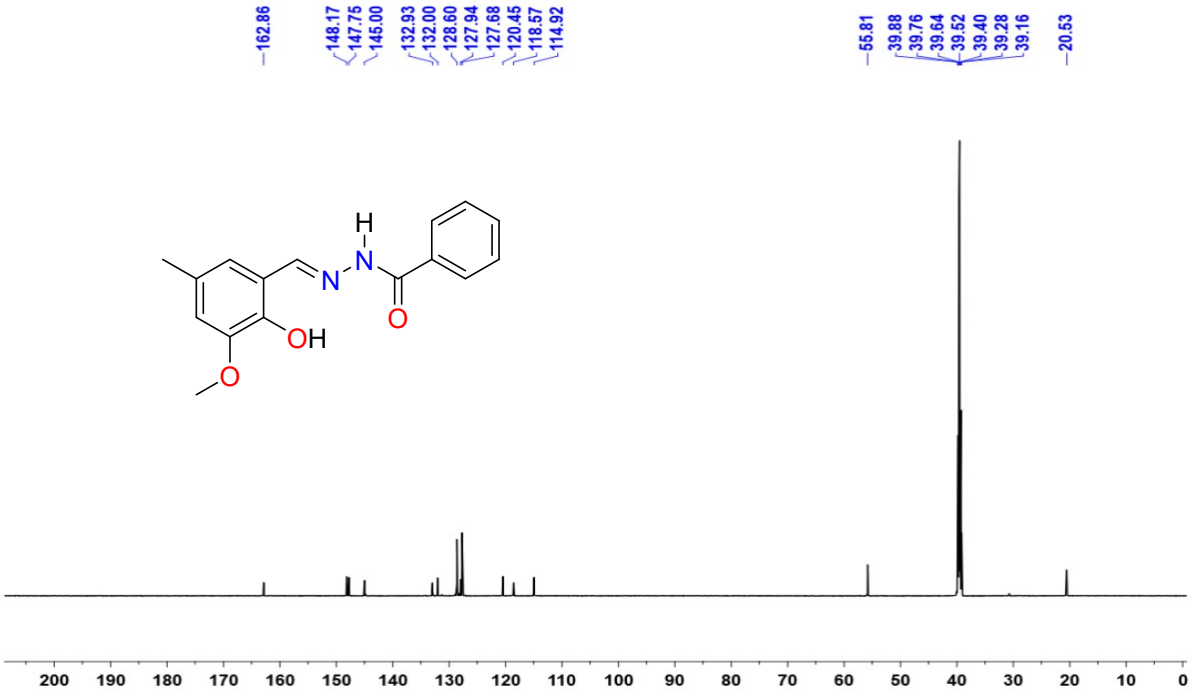

Fig. S3: ^{13}C NMR of *N'*-(2-hydroxy-3-methoxy-5-methylbenzylidene)benzohydrazide (H_2L^1) in DMSO d_6 at r.t..

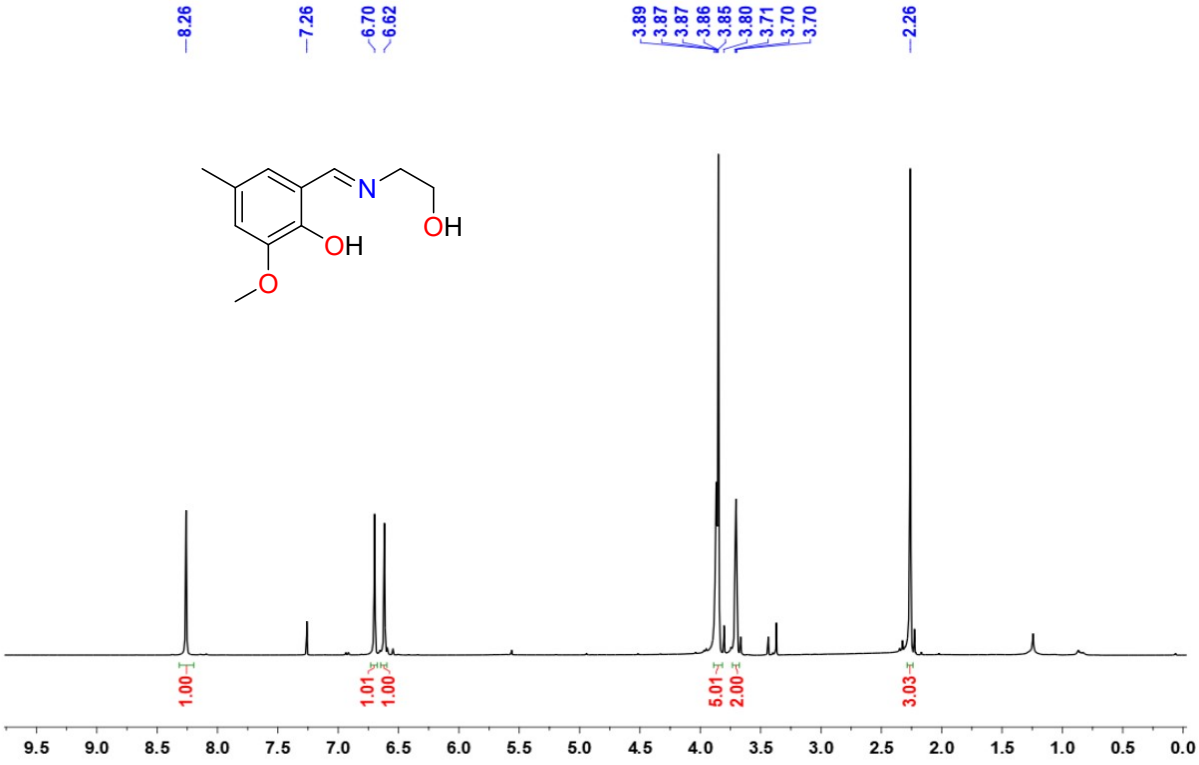

Fig. S4: ^1H NMR of 2-[(2-hydroxyethylimino)methyl]-6-methoxy-4-methylphenol (H_2L^2) in $CDCl_3$ at r.t.

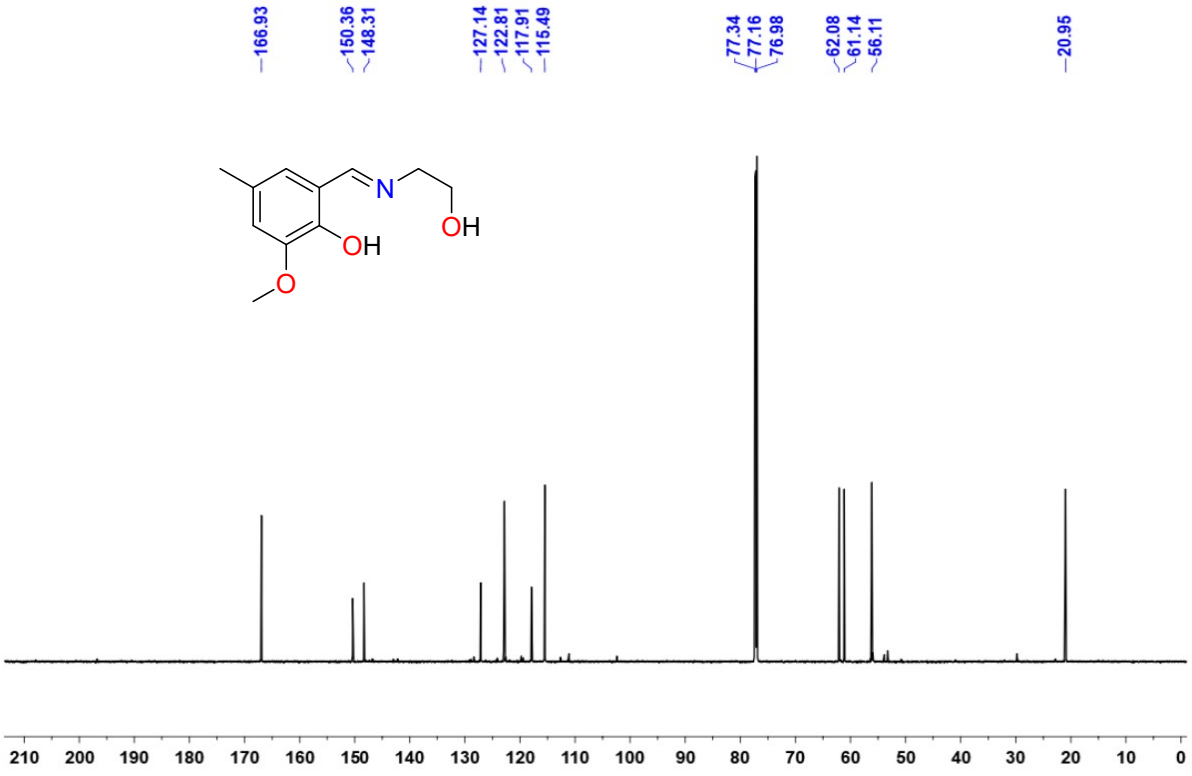

Fig. S5: ^{13}C NMR of 2-[(2-hydroxyethylimino)methyl]-6-methoxy-4-methylphenol (H_2L^2) in $CDCl_3$ at r.t.

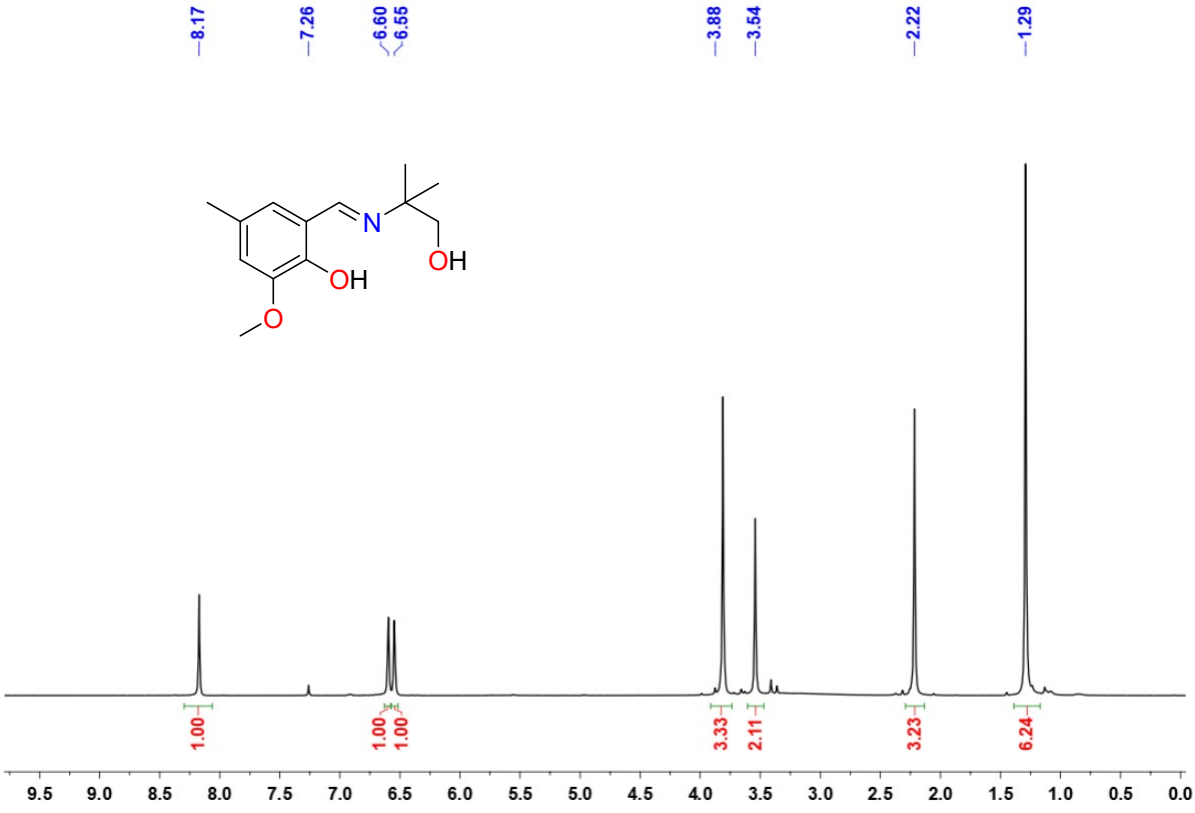

Fig. S6: ^{1}H NMR of 2-[(1-hydroxy-2-methylpropan-2-ylimino)methyl]-6-methoxy-4-methylphenol (H_2L^3) in $CDCl_3$ at r.t.

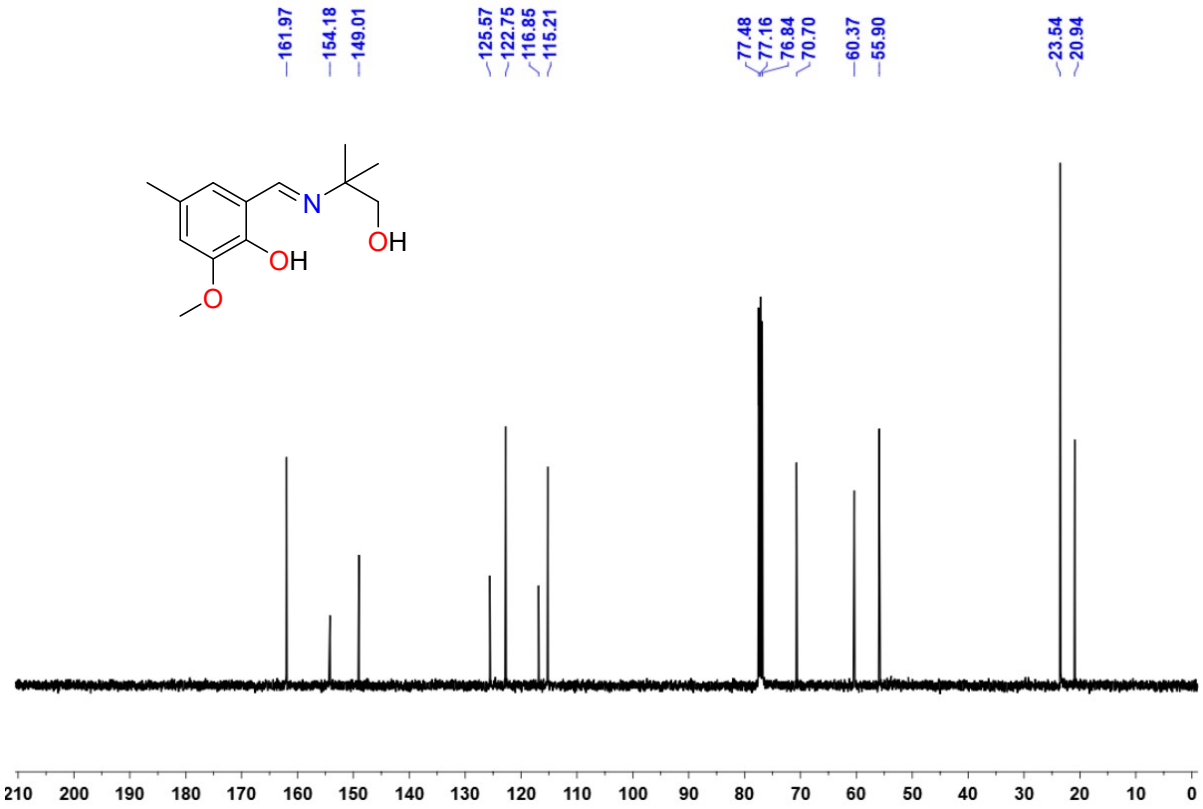

Fig. S7: ^{13}C NMR of 2-[(1-hydroxy-2-methylpropan-2-ylimino)methyl]-6-methoxy-4-methylphenol (H_2L^3) in $CDCl_3$ at r.t.

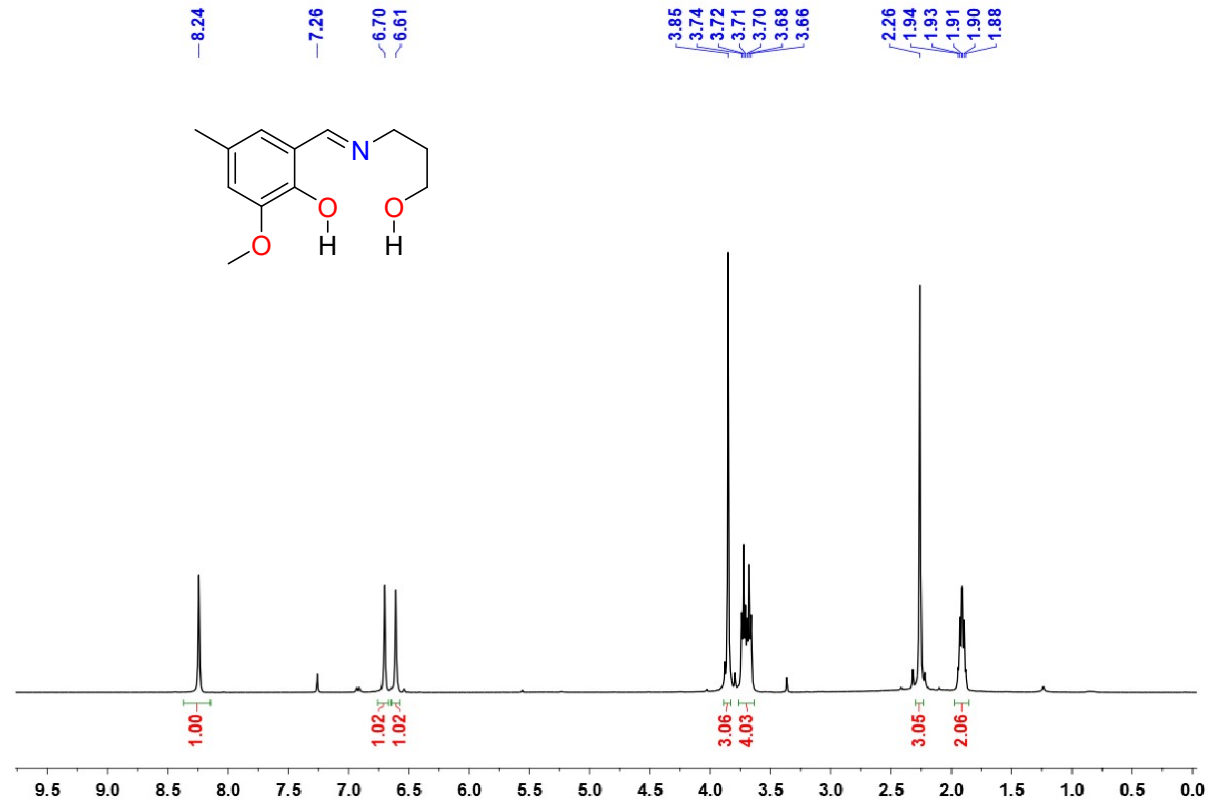

Fig. S8: ^1H NMR of 2-[(3-hydroxypropylimino)methyl]-6-methoxy-4-methylphenol (H_2L^4) in $CDCl_3$ at r.t.

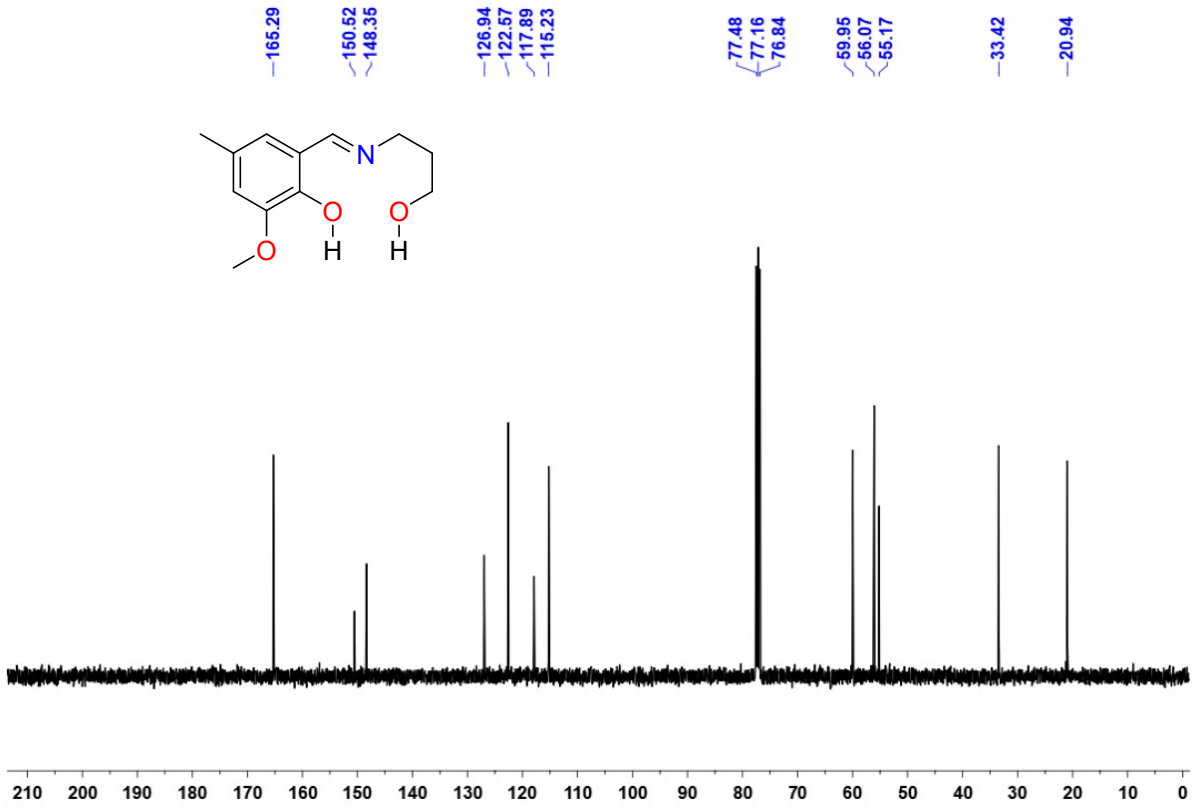

Fig. S9: ^{13}C NMR of 2-[(3-hydroxypropylimino)methyl]-6-methoxy-4-methylphenol (H_2L^4) in $CDCl_3$ at r.t.

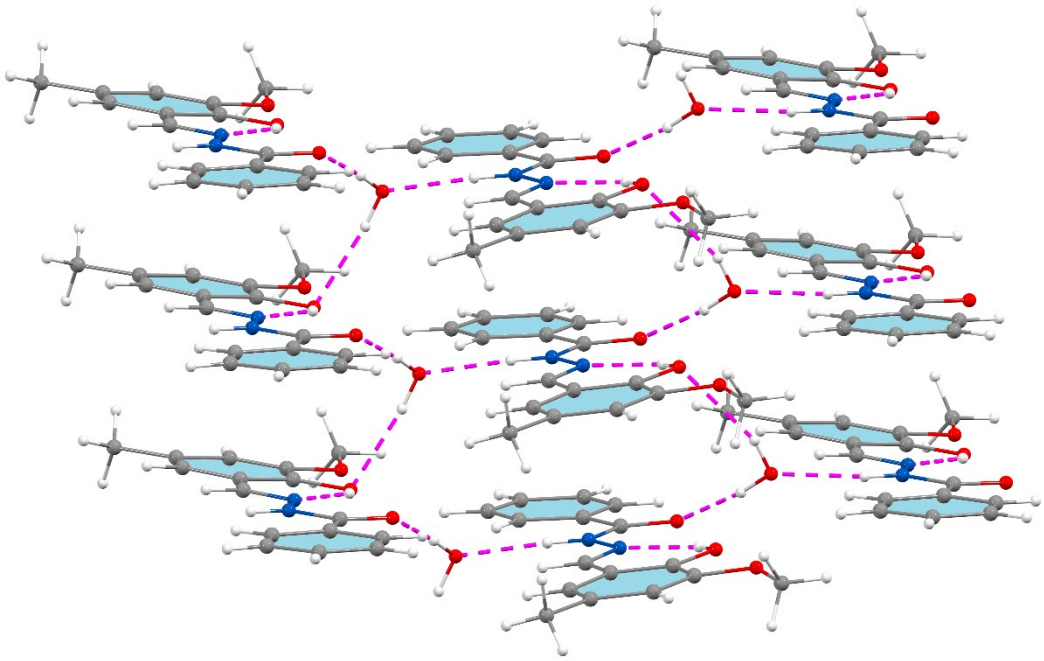

Fig. S10. Crystal packing of Schiff base H_2L^1.

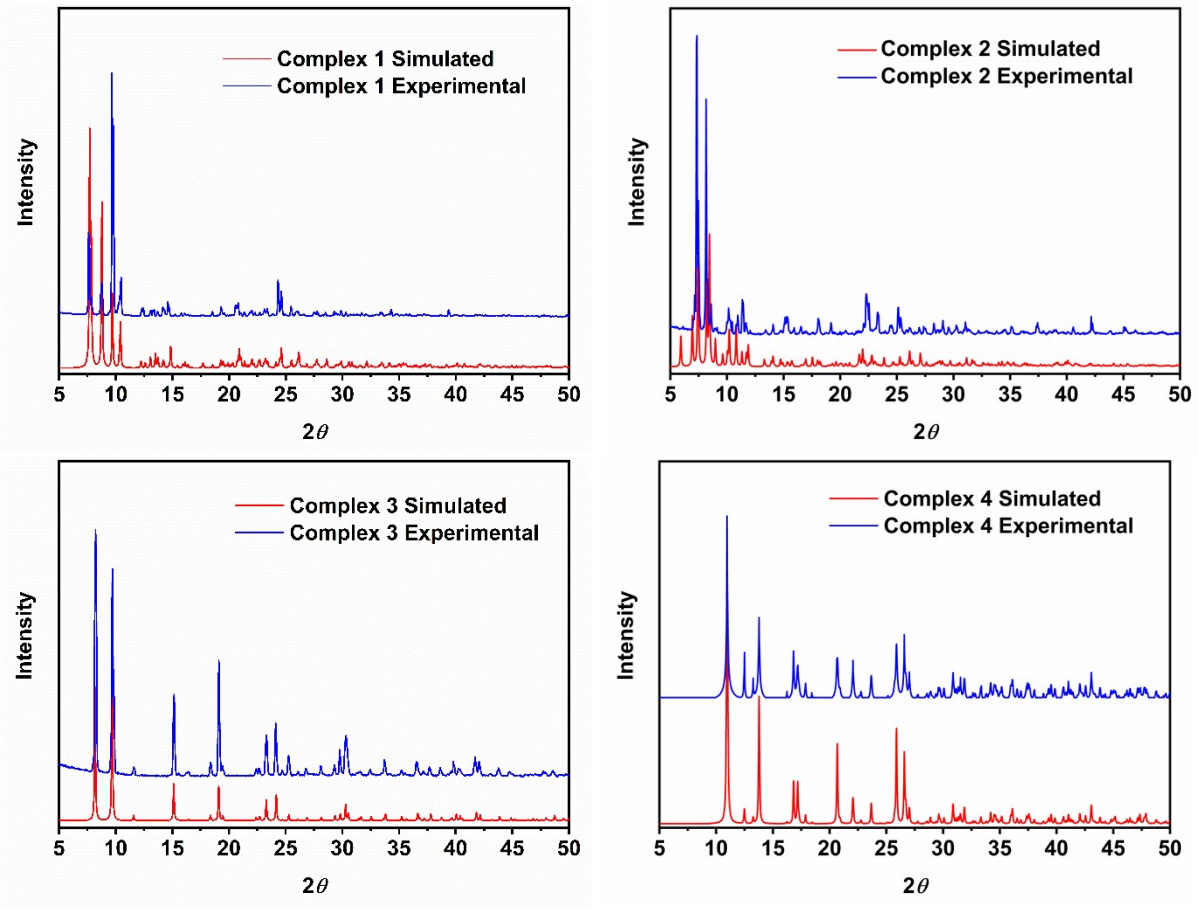

Fig. S11: Simulated and experimental powder X-ray data of the complexes.

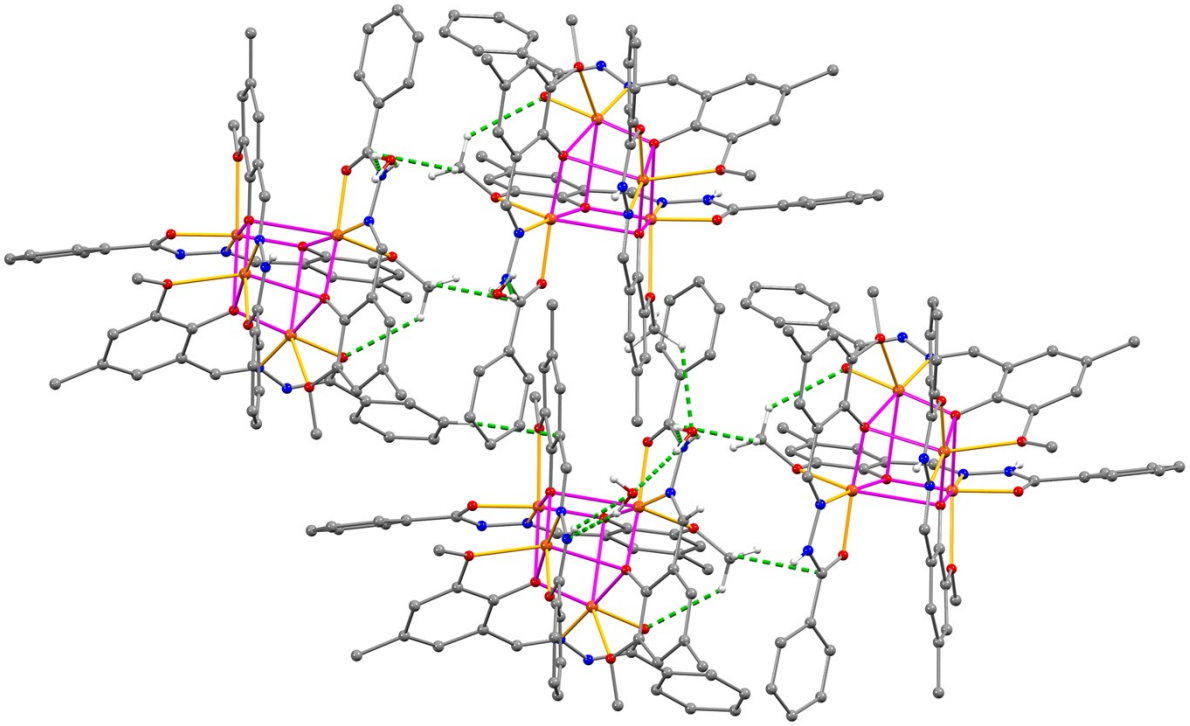

Fig. S12. A part of crystal packing in complex **1** displaying various hydrogen bonding with solvated water molecule and C−H···π interactions.

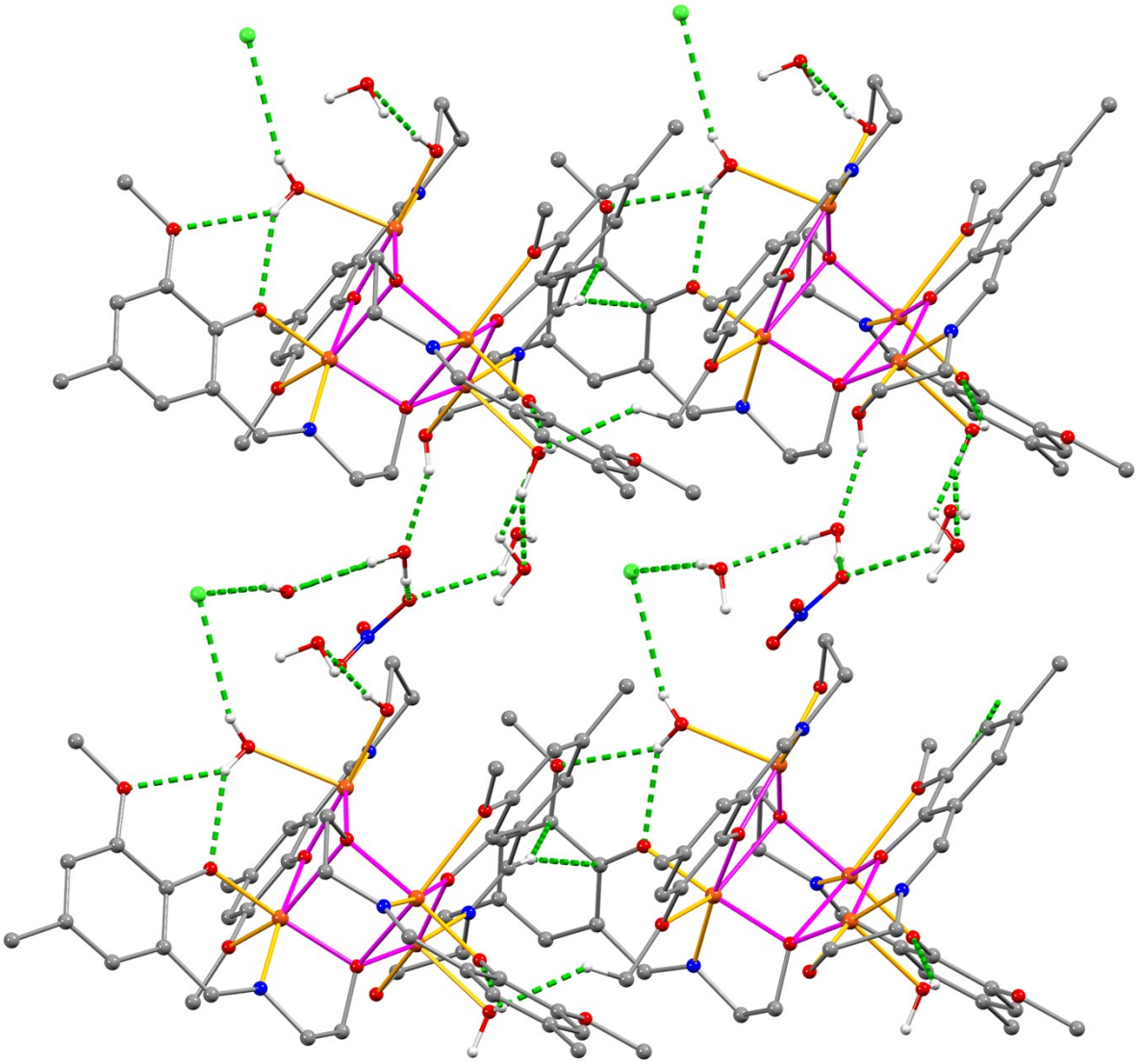

Fig. S13. A part of crystal packing in complex **2** displaying various hydrogen bonding with solvated water molecule and C−H···π interactions.

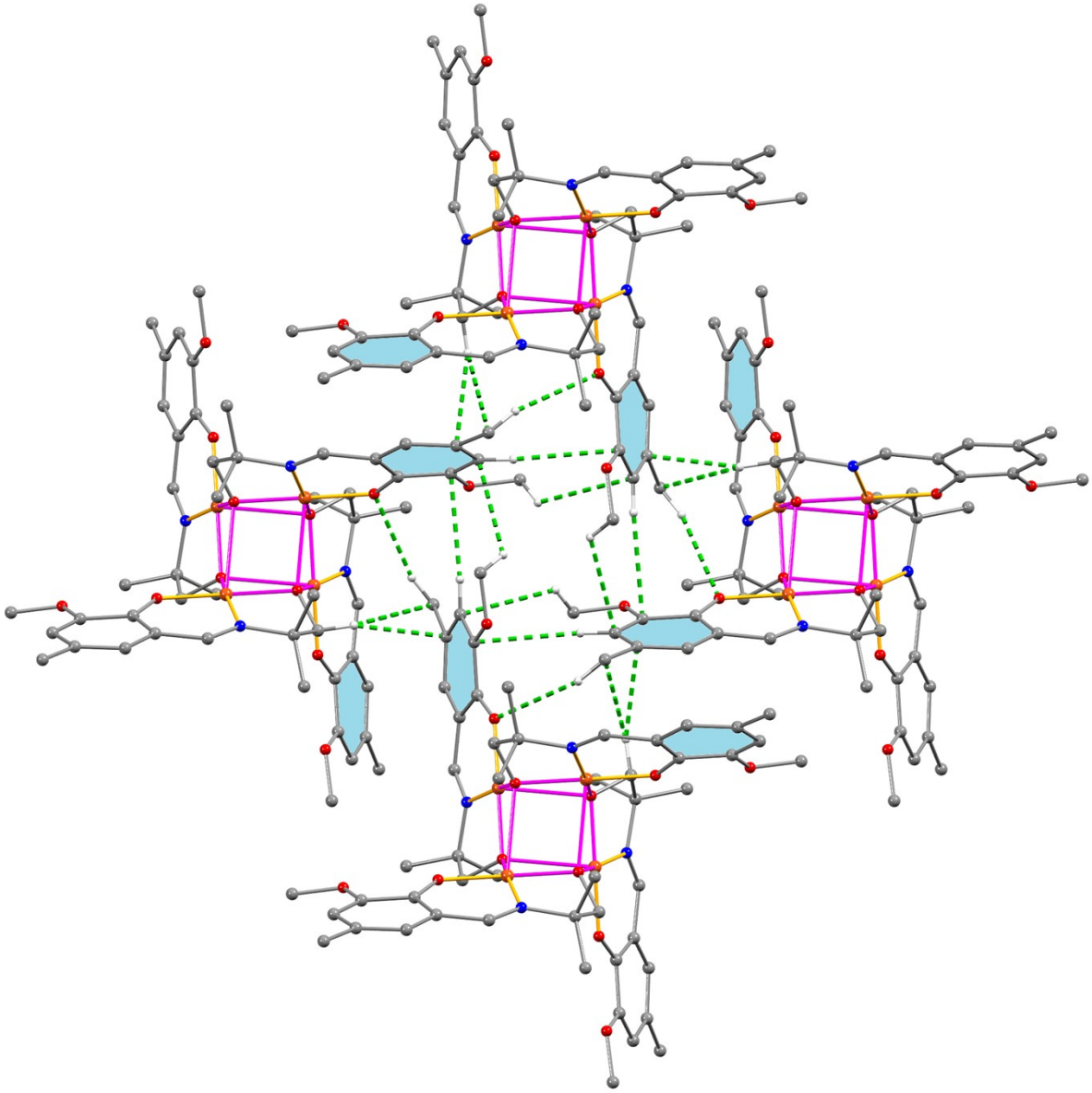

Fig. S14. A part of crystal packing in complex **3** displaying π–π stacking and C–H···π interactions.

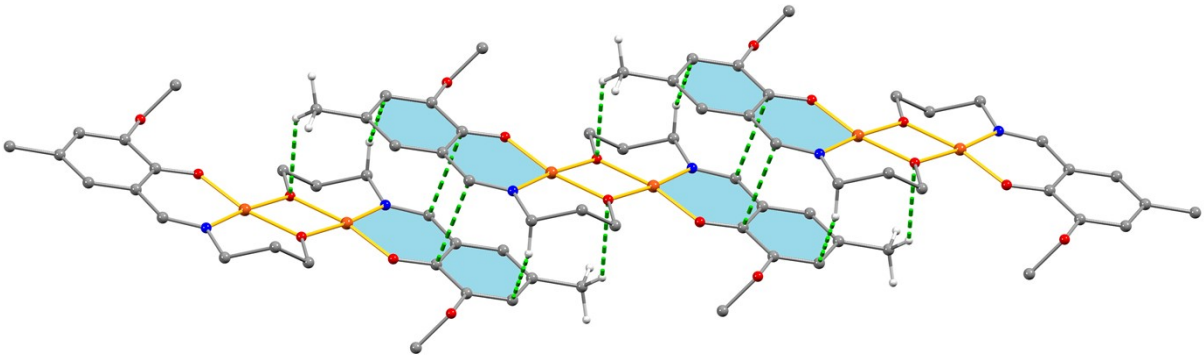

Fig. S15. A part of crystal packing in complex **4** displaying π–π stacking and C–H···π interactions.

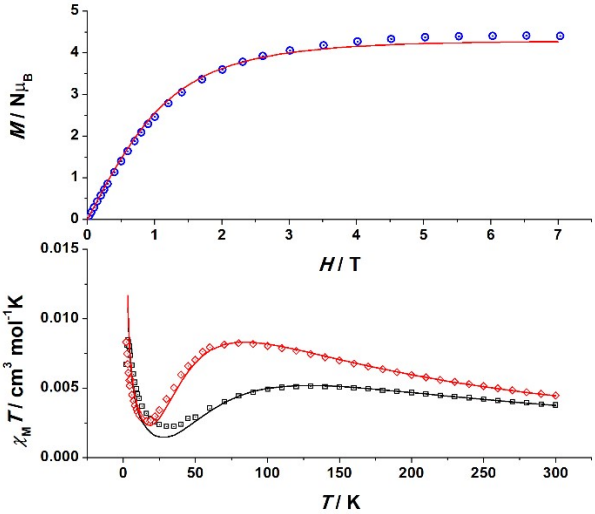

Fig. S16. Top, magnetization plot for complex **3**, measured at 2 K. Bottom, susceptibility versus temperature plot for complexes **1** (red diamonds) and **2** (black squares. Solid lines show the best fit of the data).

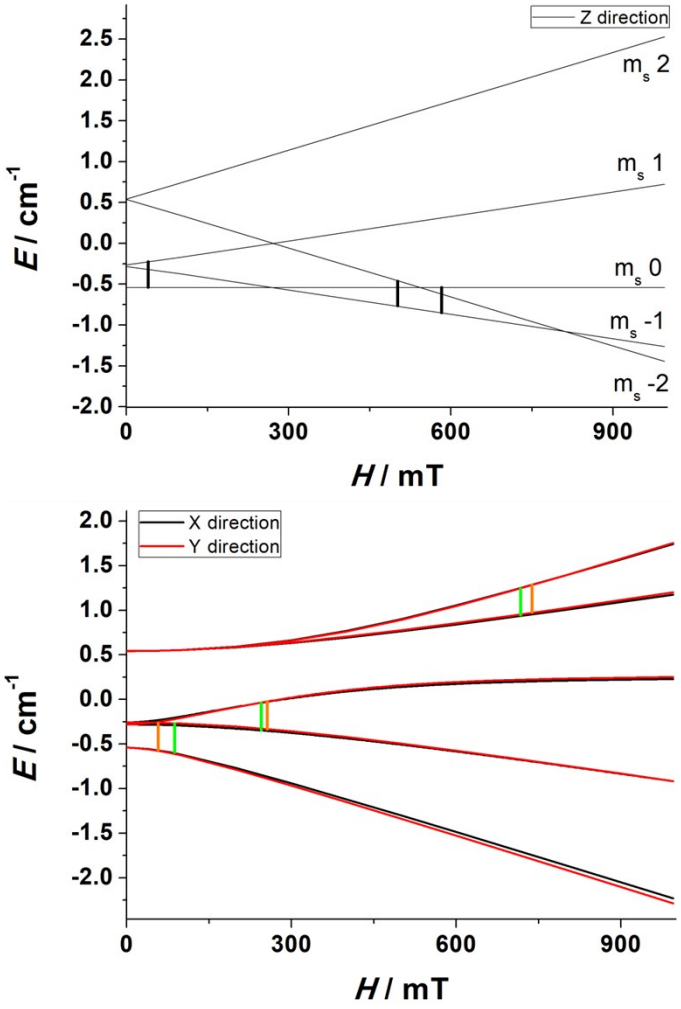

Fig. S17: Zeeman splitting of the ground spin state of complex **3** along the three main axis showing the allowed EPR transitions.

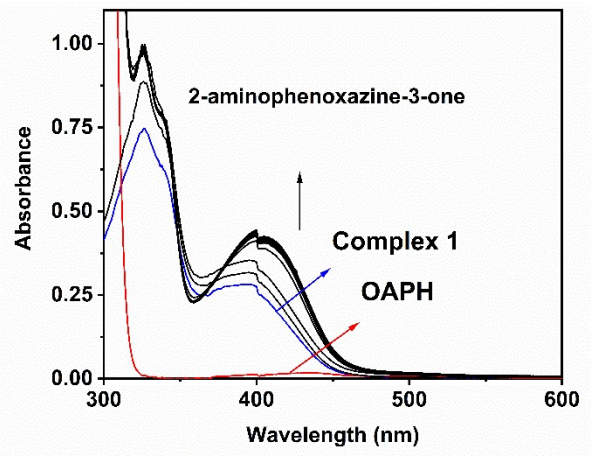

Fig. S18: UV-vis spectral scans for the biomimetic oxidation of *o*-aminophenol (OAPH) showing the negligible oxidation for the complexes **1**.

Table S1. Crystal data and structure refinement for Schiff base H_2L^1 and complexes **1–4**.

Identification code	**H_2L^1**	Complex-1	**2**	**3**	**4**
Empirical formula	$C_{16}H_{18}N_2O_4$	$C_{64}H_{59}Cu_4N_8O_{13.5}$	$C_{44}H_{66}ClN_5O_{21}Cu_4$	$C_{52}H_{68}N_4O_{12}Cu_4$	$C_{12}H_{15}NO_3Cu$
Formula weight	302.32	1410.35	1290.62	1195.26	284.79
Temperature/K	150	100	150	150	150
Crystal system	orthorhombic	orthorhombic	monoclinic	tetragonal	monoclinic
Space group	$P2_12_12_1$	Aea2	$P2_1/c$	$I\bar{4}$	$P2_1/c$
a/Å	4.86772(10)	36.4484(7)	11.9803(8)	15.2634(9)	8.89510(10)
b/Å	13.6394(2)	23.7380(4)	25.4313(17)	15.2634(9)	12.8395(2)
c/Å	22.0354(4)	14.0430(3)	18.5445(13)	11.3683(11)	10.8447(2)
α/°	90	90	90	90	90
β/°	90	90	98.038(2)	90	107.378(1)
γ/°	90	90	90	90	90
Volume/Å^3	1462.99(5)	12150.2(4)	5594.5(7)	2648.5(4)	1182.02(3)
Z	4	8	4	2	4
ρ_{calc}g/cm^3	1.373	1.542	1.532	1.499	1.600
μ/mm^{-1}	0.824	1.454	1.625	1.648	1.842
F(000)	640.0	5784.0	2664.0	1240.0	588.0
Radiation	Cu Kα (λ = 1.54184)	MoKα (λ = 0.71073)	MoKα (λ = 0.71073)	MoKα (λ = 0.71073)	MoKα (λ = 0.71073)
2Θ range for data collection/°	3.811 to 77.795	4.044 to 59.296	3.788 to 52.806	5.338 to 50.692	4.798 to 58.304

Reflections collected	8671	61970	60266	44800	26264
Independent reflections	2943 [R_{int} = 0.0512, R_{sigma} = 0.0485]	13458 [R_{int} = 0.0575, R_{sigma} = 0.0440]	11438 [R_{int} = 0.0396, R_{sigma} = 0.0319]	2403 [Rint = 0.0413, Rsigma = 0.0155]	3031 [Rint = 0.0327, Rsigma = 0.0171]
Data/restraints/parameters	2943/3/212	13458/934/924	11438/62/714	2403/0/168	3031/0/156
Goodness-of-fit on F^2	1.067	1.035	1.024	1.065	1.045
Final R indexes [I>2σ (I)]	R_1 = 0.0364, wR_2 = 0.0953	R_1 = 0.0478, wR_2 = 0.1045	R_1 = 0.0522, wR_2 = 0.1521	R_1 = 0.0156, wR_2 = 0.0428	R_1 = 0.0203, wR_2 = 0.0531
Final R indexes [all data]	R_1 = 0.0393, wR_2 = 0.0974	R_1 = 0.0602, wR_2 = 0.1111	R_1 = 0.0720, wR_2 = 0.1668	R_1 = 0.0163, wR_2 = 0.0432	R_1 = 0.0222, wR_2 = 0.0541
Largest diff. peak/hole / e $Å^{-3}$	0.18/-0.24	0.67/-0.38	2.48/-0.57	0.39/-0.16	0.35/-0.25
Flack parameter	0.08(16)	-0.013(12)	-	0.013(13)	-

Table S2. Bond distances (in Å) and angles (º) for complex **4**.

Parameters	4
Cu1−O1	1.8930(8)
Cu1−O3^1	1.9359(8)
Cu1−O3	1.9184(8)
Cu1−N1	1.9453(10)
Cu1···Cu1^1	3.0494(3)
Cu1−O3−Cu1^1	104.59(4)

Symmetry code: ^{1}-X,1-Y,1-Z

Table S3. Calculated energy for the spin levels of the ferromagnetic complex **3** and their population at low temperature.

Spin	Energy (cm^{-1})	Population at 2K
2.0	0.00	100.00
0.0	65.84	0.00
1.0	65.84	0.00
1.0	65.84	0.00
1.0	131.68	0.00
0.0	197.52	0.00